Mater Eng Res, 2021, 3(1): 133-143
DOI: 10.25082/MER.2021.01.002

RESEARCH ARTICLE

Structural, electrical, and magnetic characterization of (1-*x*)$BaTiO_3$-*x*$Ni_{0.6}Zn_{0.4}Fe_2O_4$ multiferroic ceramic composites

Golam Mowla[1] **Nabid Hossain**[1] **M. Humayan Kabir**[1*] **M. Jahidul Haque**[1] **M. Mintu Ali**[1] **M. Abdul Kaiyum**[1] **M. S. Rahman**[1]

[1] Department of Glass & Ceramic Engineering, Rajshahi University of Engineering & Technology (RUET), Rajshahi 6204, Bangladesh

Check for updates

Correspondence to: M. Humayan Kabir, Department of Glass & Ceramic Engineering, Rajshahi University of Engineering & Technology (RUET), Rajshahi 6204, Bangladesh; Email: mhk.gce11@gmail.com

Received: May 22, 2021;
Accepted: July 21, 2021;
Published: July 23, 2021.

Citation: Mowla G, HossainN, Kabir MH, *et al*. Structural, electrical, and magnetic characterization of (1-*x*)$BaTiO_3$-*x*$Ni_{0.6}Zn_{0.4}Fe_2O_4$ multiferroic ceramic composites. *Mater Eng Res*, 2021, **3**(1): 133-143. https://doi.org/10.25082/MER.2021.01.002

Copyright: © 2021 M. Humayan Kabir *et al*. This is an open access article distributed under the terms of the Creative Commons Attribution License, which permits unrestricted use, distribution, and reproduction in any medium, provided the original author and source are credited.

Abstract: In the present work, pure $BaTiO_3$, pure $Ni_{0.6}Zn_{0.4}Fe_2O_4$ and (1-x)$BaTiO_3$-x$Ni_{0.6}Zn_{0.4}Fe_2O_4$ (where x = 0.15, 0.25 & 0.35) multiferroic composites were synthesized through solid-state sintering scheme. Structural, microstructural, ferroelectric, and ferromagnetic analysis was performed. Both tetragonal perovskite phase (for $BaTiO_3$ferroelectric phase) and cubic spinel ferrite phase (for $Ni_{0.6}Zn_{0.4}Fe_2O_4$ ferromagnetic phase) were simultaneously presented within each composite. The ferrite phase exhibited a smaller crystallite size compared to the ferroelectric phase. All of the composites demonstrated homogenous irregular-shaped grains. The measured average grain size for 0.85$BaTiO_3$-0.15$Ni_{0.6}Zn_{0.4}Fe_2O_4$, 0.75$BaTiO_3$-0.25$Ni_{0.6}Zn_{0.4}Fe_2O_4$, 0.65$BaTiO_3$-0.35$Ni_{0.6}Zn_{0.4}Fe_2O_4$were 364.14 nm, 378.46 nm and 351.62nm, whereas the density values were 3.04g/cm^3, 3.20g/cm^3 and 3.13 g/cm^3 for x = 0.35, 0.25, 0.15 respectively. However, the heterogenous microstructure was observed for all of the compositions. The composites exhibited an oval-shaped lossy capacitor hysteresis loop. However, 0.75$BaTiO_3$-0.25$Ni_{0.6}Zn_{0.4}Fe_2O_4$composite showed the highest remnant polarization (11.613 μC/cm^2) and coercive field value (1.526 kV/cm), ensuring its usability for switching applications. In addition, 0.75$BaTiO_3$-0.25$Ni_{0.6}Zn_{0.4}Fe_2O_4$also exhibited the maximum saturation (M_s= 1.732 emu/g) and remnant magnetization (M_r= 0.025 emu/g) among the composites. Nevertheless, all of the composites derived 'wasp-waisted' hysteresis loops due to the presence of either superparamagnetic (SPM) particles or a mixer of a single domain (SD) and superparamagnetic particles.

Keywords: multiferroic, ferroelectric, magnetic, SPM component

1 Introduction

Multiferroic materials have attracted huge interest among researchers in the last decades due to their huge prospective appliances in multifunctional devices [1]. Ferroelectric materials have wide prospective applications in the electronic sector in manufacturing actuators, non-volatile memories, sensors, capacitors, transducers, data storage, capacitive/inductive passive filters for telecommunications as a range of other applications [2–4]. According to the literature, it was H. Schmid who first used the phrase 'Multiferroic' in 1994. Modern definitions denote materials that demonstrate at least two ferroic characteristics (ferroelectricity, ferromagnetism, and ferroelasticity) at the same time. Consequently, they exhibit spontaneous polarization in the presence of an applied magnetic field and exhibit spontaneous magnetization in an external electric field [5]. There have two types of multiferroic materials: single-phase and composites consisting of two or more phases [5,6]. In single-phase materials, there have many problems like inherent weak coupling between the order's parameters at and above room temperature, lower magnetization intensity, lack of scope of tuning magnetoelectric response, weak magnetoelectric coupling coefficient as well as large leakage current density. Moreover, they can be expensive and burdened with the degradation with repeated usage, resulting in their usage impractical in device applications [6–8]. Due to these unavoidable adversative aspects, multiphase or ceramic material has become the current focus of attention in the scientific community as it has the potential to resolve these limitations [7]. Ce-Wen Nan et al. [6] showed that multiphase multiferroic's magnetoelectric effect isa hundred times larger than those found in single-phase multiferroic one. The effective magnetoelectric effects in composites, including magnetostriction as well as piezoelectric co-efficient of the ferroelectric phase as well as ferrite phase along with poling strength, high dielectric permeability as well as a molar percentage; furthermore, the chemical

reaction shouldn't take place between the comprised phrases, and both phases should have high resistivity to avert the leakage of accumulated charge [9]. However, multiphase materials have the following advantages: Improved piezoelectric properties, high dielectric permittivity; they are relatively cheaper, easier to fabricate, possess superior magnetoelectric coupling response at ambient temperature, and tailoring of properties of these composite are comparatively easy [8, 10]. As the multiferroics demonstrate improved characteristics and exhibit a higher magnetoelectric effect than single phases composites, they are gaining huge popularity [4]. A wide variety of magnetoelectric bulk materials have been fabricated and studied in the modern literature including $BaSrTiO_3$-$NiZnFe_2O_4$, $BaTiO_3$-(Ni-Zn)Fe_2O_4, $CoFe_2O_4$-$BaTiO_3$, $Ba_{0:6}Sr_{0:4}TiO_3$–$Ni_{0.8}Zn_{0.2}Fe_2O_4$, Ni(Co,Mn)Fe_2O_4-$BaTiO_3$, $NiZnFe_2O_4$–PZT, , $NiFe_2O_4$-$BaTiO_3$, $BaTiO_3$–$CoFe_2O_4$, Ni(Cu,Zn)Fe_2O_4-$BaTiO_3$, x$NiFe_2O_4$–(1-x) $BaTiO_3$etc [1, 2, 5]. Recently, various magnetoelectric bulk composites have been produced and investigated, such as x$NiFe_2O_4$–(1-x) $BaTiO_3$, etc. [1, 2, 5]. Among the multiferroic composite system, $BaTiO_3$-(Ni-Zn)Fe_2O_4 composite has attracted more attention because of its environmental friendliness and the coexistence of the novel magnetoelectric coupling effect, high electrical resistivity, high permittivity, chemical stability as well as excellent electromagnetic properties, low dielectric loss, etc. [11, 12]. The composite of $BaTiO_3$-(Ni:Zn)Fe_2O_4 possesses superior properties due to the coexistence of $BaTiO_3$and NiZn ferrite phases. It is known that $BaTiO_3$ has a tetragonal perovskite structure which represents the ferroelectric materials and has high dielectric constant, high permittivity, low dielectric loss, low leakage current density, and high tunability [5, 10]. Ni-Zn ferrite is spinel ferrite, represents the ferromagnetic materials with superior soft magnetic materials, committed its high permeability, greater electrical resistivity, the high value of magnetization, and high chemical stability, high curie temperature [5, 7, 10, 11]. Zhi Yu et al. suggested that by incorporating these two composites into a composite, the composite could've exhibited some exciting magnetic/electric properties [10]. Moreover, fine, homogeneous nanosized powders are necessary to develop desired properties and for practical applications of the multiferroics composites [13, 14]. However, nanoparticles exhibit different properties due to various fabrication methods as well as sintering conditions. Hence, choosing the appropriate synthesis method is very significant to attain the ferrite nanoparticles [14]. In recent times, numerous techniques have been developed to fabricate the multiferroics successfully. Some of the most popular techniques include solid-state sintering, sol-gel processing, co-precipitation, hydrothermal synthesis or other wet chemical fabrication techniques [12, 14]. Among them, the hydrothermal method is very flexible. But one of the main drawbacks of the hydrothermal method is the slow reaction kinetics at any given temperature [15]. Despite having several advantages, the sol-gel process also has several drawbacks, for instance, longer reaction time, aggregation & agglomeration, and the complexities in adjusting the particle size [16]. Co-precipitation, another conventional method also used to synthesis multiferroics. In this method, the controlling of the particle size and size distribution is very difficult and also very often, fast (uncontrolled) precipitation takes place during synthesis of multiferroics [17]. As compared to other synthesis method, we have chosen solid state synthesis method to synthesis $BaTiO_3$-(Ni:Zn)Fe_2O_4 nanoparticles. The alleged solid–solid reaction is a mechanochemical method which transpires between powders in the solid state. The reason of choosing this method is due to its versatile advantages like: relatively simple and cost effective, reduced pollution, simplicity in process and handling, uniform particle size distribution, controllable size and capable of large scale production of nano-powders [18–20]. Generally it is needed higher annealing and sintering temperature to synthesis the $BaTiO_3$-(Ni:Zn)Fe_2O_4composite by solid state synthesis methods. To the best of our knowledge most of the authors who synthesized $BaTiO_3$-(Ni:Zn)Fe_2O_4composites, they used around (1050-1200°C) temperature to calcine their sample and used around (1120-1325°C) temperature to sinter their samples [1, 5, 10–12, 21]. However, in our present work we have taken an attempt to synthesis $BaTiO_3$-$Ni_{0.6}Zn_{0.4}Fe_2O_4$ (where $BaTiO_3$& $Ni_{0.6}Zn_{0.4}Fe_2O_4$ ratios are: 65:35, 75:25 & 85:15 mol% respectively) nanoparticles using lower calcination & sintering temperature to investigate the structural, morphological, dielectric, ferroelectric as well as magnetic properties of the composites.

2 Materials and methods

Pure $BaTiO_3$ [BTO], pure $Ni_{0.6}Zn_{0.4}Fe_2O_4$ [NZFO], (1-x)$BaTiO_3$-x$Ni_{0.6}Zn_{0.4}Fe_2O_4$, (where x = 0.15, 0.25 & 0.35) composites were prepared by solid-state synthesis route. To prepare $BaTiO_3$-$Ni_{0.6}Zn_{0.4}Fe_2O_4$composites i.e. [0.85$BaTiO_3$-0.15$Ni_{0.6}Zn_{0.4}Fe_2O_4$ (0.85BTO-0.15NZFO), 0.75$BaTiO_3$-0.25$Ni_{0.6}Zn_{0.4}Fe_2O_4$ (0.75BTO-0.25NZFO), 0.65$BaTiO_3$-0.35$Ni_{0.6}$ $Zn_{0.4}Fe_2O_4$ (0.65BTO-0.35NZFO)], first $BaTiO_3$ (BTO) and $Ni_{0.6}Zn_{0.4}Fe_2O_4$ (NZFO) nanopowders were synthesized individually and then were mixed in proper ratio. Barium carbonate

[$BaCO_3$, purity > 99%, Merck Specialties, India] and titanium dioxide [TiO_2, purity > 99%, Merck Specialties, India] powder was used as a source material of $BaTiO_3$. Subsequently, Nickel oxide [NiO, purity > 99%, Merck Specialties, India], zinc oxide [ZnO, purity > 99%, Merck Specialties, India]&ferric oxide [Fe_2O_3, purity > 99%, Merck Specialties, India] were used as a source for nickel-zinc ferrite ($Ni_{0.6}Zn_{0.4}Fe_2O_4$) nano-powder. For the preparation of $BaTiO_3$, Proper amounts of barium carbonate and titanium dioxide powders were weighed, and the ball milled for 20 hours using an adequate amount of ethanol medium. The ball-milled solution was then dried and crushed. The obtained powder was then calcined at 900°C for 3 hours. Similar steps were followed to prepare the nickel-zinc ferrite powder. Then, $BaTiO_3$ and $Ni_{0.6}Zn_{0.4}Fe_2O_4$ (Three different batches where $BaTiO_3$& $Ni_{0.6}Zn_{0.4}Fe_2O_4$ ratios are as follows: 65:35, 75:25 & 85:15 mol%, respectively) powders along with a sufficient amount of ethanol were taken into ball mill to mix the powder properly. After ball milling, the powder was finely crushed to get the homogeneous powder with the desired composition. Afterward, the mixed powder was pressed into a pellet presser to make pellets. The average diameter and thickness of all pellets were about 1.532 cm and 0.173 cm, respectively. Finally, all the pellets were then sintered at 1050°C for 3 hours. The composites' structural phasewas investigated using theX-ray diffraction (XRD) technique using Bruker D8 advanced diffractometer (λ = 1.5406 Å). The surface morphology of the samples was revealed by EVO-18 research scanning electron microscope (SEM). The ferroelectric properties were observed by a P-E loop tracer multiferroic tester (model: P-PMF, Radiant Tech. Inc. USA). Finally, the magnetic properties were analyzed using a vibrating sample magnetometer (model: (VSM, EV-9, MicroSense).

3 Result and Discussion

3.1 Structural analysis

The X-ray diffraction spectrograph of pure $BaTiO_3$, $Ni_{0.6}Zn_{0.4}Fe_2O_4$ and (1-x)$BaTiO_3$-x$Ni_{0.6}Zn_{0.4}Fe_2O_4$ (where x = 0.15, 0.25 & 0.35) composites are displayed in Figure 1(a-e).

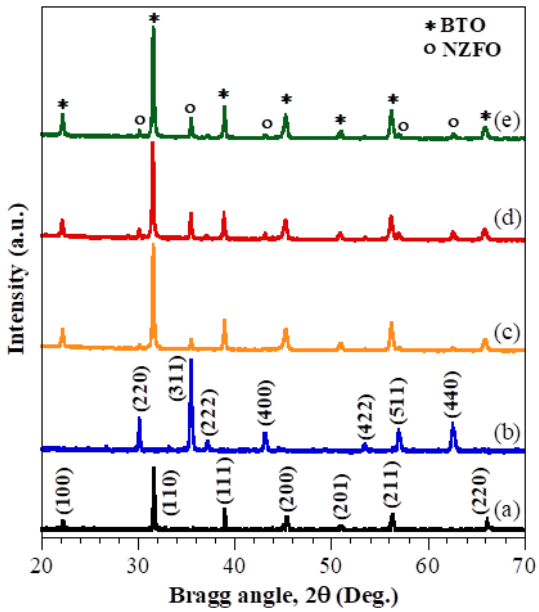

Figure 1 X-ray diffraction spectrograph of (a) BTO, (b) NZFO, (c) 0.85BTO-0.15NZFO, (d) 0.75BTO-0.25NZFO, (e) 0.65BTO-0.35NZFO.

Figure 1(a) & (b) observed that the BTO has a tetragonal perovskite structure while the NZFO has a cubic spinel structure. The diffraction peaks of BTO have good agreement with JCPDS cards no. 86-1570 and NZFO matches with JCPDS cards no 52-0277. Therefore, the nonexistence of the secondary or impurity phase confirms the successful synthesis of BTO& NZFO. All peaks correspond to BTO, and NZFO phases are identified from (1-x)$BaTiO_3$-x$Ni_{0.6}Zn_{0.4}Fe_2O_4$ composite systems as shown in Figure 1(c-e) confirms the successful formation of bi-phasic composite, i.e., the composites consist of BTO as ferroelectric and NZFO as a ferromagnetic phase.

The crystal size (D) of the composites has been measured by using Scherer's equation [8]:

$$D = \frac{0.9\lambda}{\beta \cos\theta} \quad (1)$$

Where λ is the wavelength of X-ray and iβs the full width at half maxima of the sharpest peak. The calculated values are tabulated in Table 1. It is observed that the ferrite phase's grain size is smaller than that of the ferroelectric phase into the composites.

Table 1 Calculated lattice parameters and crystallite size of (1-x)$BaTiO_3$-x$Ni_{0.6}Zn_{0.4}Fe_2O_4$ composites

Composition	Lattice parameters ($\AA$)				Crystallite size, D (nm)	
	Ferrite phase	Ferroelectric phase			Ferrite	Ferroelectric
	a	a	c	c/a		
BTO	-	3.9993	4.0052	1.0015		73.76
NZFO	8.3930	-	-	-	62.72	
0.85BTO-0.15NZFO	8.3901	4.0081	4.0086	1.0001	72.45	74.27
0.75BTO-0.25NZFO	8.399	4.0146	4.0113	0.9992	68.66	70.73
0.65BTO-0.35NZFO	8.3899	4.008	4.0087	1.0002	68.44	71.10

From Figure 1(a) & (b), it is noticeable that the (110) peak is dominant in BTO, and (311) peak is dominant in NZFO ceramics. But in the composite system, the intensity of the (110) peak is higher, i.e., the dominant peak (110), which corresponds to the BTO phase. Therefore, it is also observed from the XRD spectrograph that the intensity of the peaks corresponds to the ferroelectric phase is stronger than the ferrite phase, i.e.,the ferroelectric phase is dominant into the (1-x)$BaTiO_3$-x$Ni_{0.6}Zn_{0.4}Fe_2O_4$ composites. This tendency may be due to the higher content of BTO in the composite.

Table 2 Calculated lattice parameters and crystallite size of (1-x)$BaTiO_3$-x$Ni_{0.6}Zn_{0.4}Fe_2O_4$ composites

Composition	Space group	Unit cell volume ($Å^3$)	Phase fraction (%)	Reliability factors (%)	GoF	Bragg R Factor	RF. Factors
0.85BTO-0.15NZFO	*P4mm*	64.56	96.74	Rp = 9.53 Rwp = 12.10 Rexp = 6.55	1.8	8.24	6.29
	Fd3m	591.55	3.26	Rp = 34.80 Rwp = 27.30 Rexp = 14.73		33.20	28.30
0.75BTO-0.25NZFO	*P4mm*	64.77	88.76	Rp = 8.42 Rwp = 11.50 Rexp = 5.17	2.2	9.30	6.17
	Fd3m	593.23	11.24	Rp = 39.90 Rwp = 32.60 Rexp = 14.67		36.70	25.90
0.65BTO-0.35NZFO	*P4mm*	64.54	89.51	Rp = 7.48 Rwp = 9.65 Rexp = 5.51	1.7	6.59	4.00
	Fd3m	591.26	10.49	Rp = 26.90 Rwp = 22.90 Rexp = 13.07		18.20	14.80

The lattice parameters of all samples have been calculated and are tabulated in Table 1. It is found that the values of lattice parameters of ferroelectric and ferrite phases are almost the same in pure and composite samples, which indicates that significant structural changes or any chemical reactions did not take place in the composites system during sintering at 1050°C.

Rietveld refinement was performed to analyze the structural transformations within the composite using the FullProf software. The refinement was carried out using *P4mm* and *Fd3m* space groups for BTO and NZFO. The observed, calculated, and different x-ray diffraction patterns are displayed in Figure 2. The refined parameters such as reliability factors [profile residual (R_p), weighed profile (R_{wp}), and expected value (R_{exp}))], the goodness of fit ($GoF = \frac{R_{wp}}{R_{exp}}$), Bragg R factor and RF factors are shown in Table 2. The unit cell volume for each phase initially paincreased up to 0.75BTO-0.25NZFO composite [BTO6 $\sim$ 4.77 $Å^3$ and NZFO $\sim$

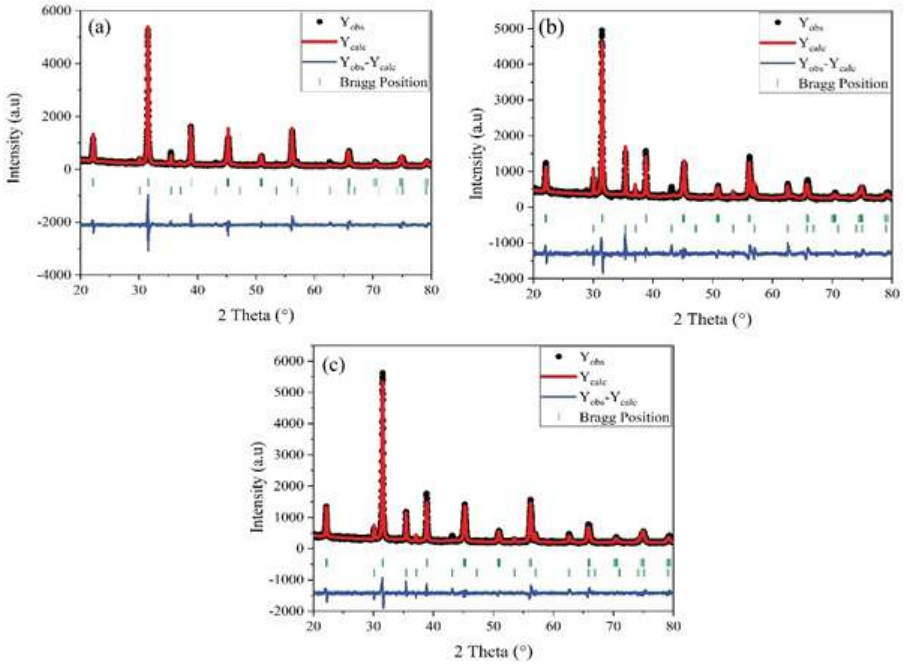

Figure 2 Rietveld refined XRD patterns of (a) 0.85BTO-0.15NZFO, (b) 0.75BTO-0.25NZFO, (c) 0.65BTO-0.35NZFO composite.

593.23 Å^3] and then decreased for 0.65BTO-0.35NZFO composite [BTO6 $\sim$ 64.54 Å^3 and NZFO $\sim$ 591.26 Å^3]. Moreover, the phase fraction value for BTO and NZFO phase also follow a similar trend.

3.2 Surface morphology (SEM)

The surface morphology of BTO, NZFO, and BTO-NZFO composites has been observed by SEM analysis. Figure 3 shows the SEM image of $BaTiO_3$ and $Ni_{0.6}Zn_{0.4}Fe_2O_4$. The BTO consists of irregularly shaped particles, whereas NZFO includes both rounds, irregular and pyramidal-shaped particles. The average grain size has been measured by linear interception method and was found 383.88 nm for BTO and 321.22 nm is for NZFO, respectively. However, the grain size of the ferroelectric phase is larger than the ferrite phase.

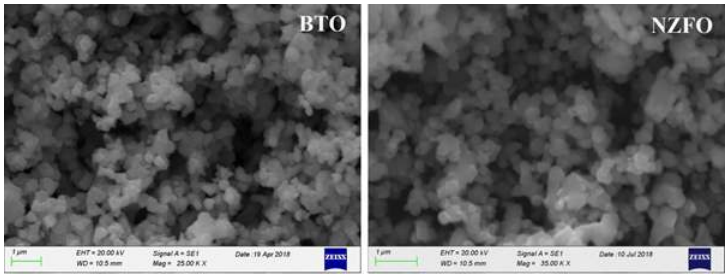

Figure 3 SEM image of pure BTO and pure NZFO

Figure 4 shows the SEM micrograph of (1-x)$BaTiO_3$-x$Ni_{0.6}Zn_{0.4}Fe_2O_4$ composites. It is observed from Figure 3 that all the composites consist of fairly homogeneous irregular shaped grains, i.e. coarse-grained particles. A. Jain et al [22] reports that coarse-grained ceramics often exhibit better piezoelectric characteristics than fine-grained ceramics. However, no agglomerations have been observed in the composites. It may be due to the lower sintering temperature of the composites. Furthermore, no porosity or cracks have been observed on the surface of the particles of the composites. However, the average grain size of the composites has also been measured by linear interception method [23] and found approximately 364.14, 378.46, and 351.62 nm when the BTO doped with 15%, 25%,and 35% NZFO, respectively. Thus, the SEM results have good agreement with the XRD. The grain size distributions have

also been calculated by using Image J software and are shown in Figure 4. It is found that all the composites consist of wide ranges of particles with different particle sizes. The presence of a wide range of particles indicates the heterogeneous microstructure. However, all the particles are in ranging from 200-600 nm.

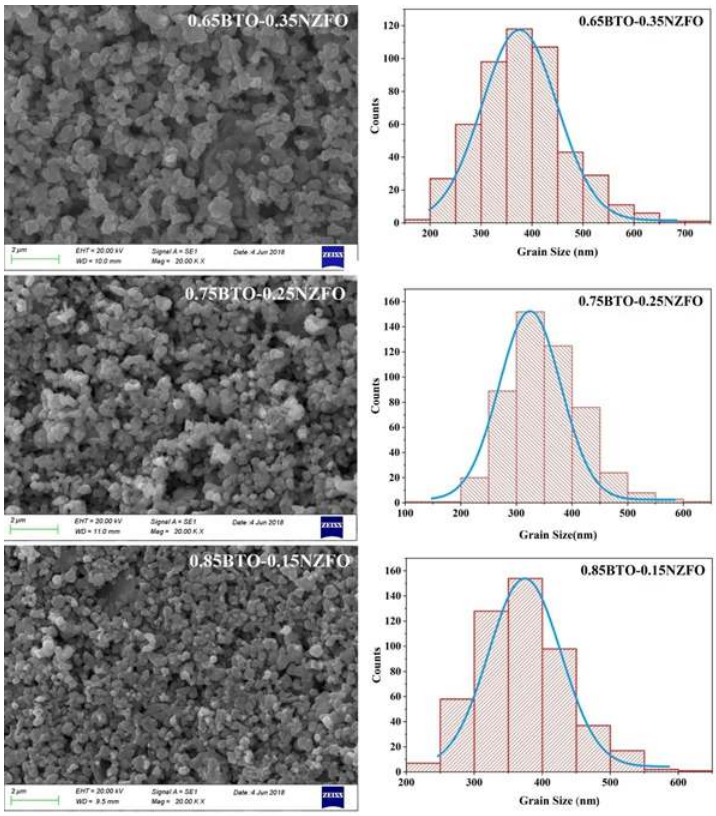

Figure 4 SEM images of (1-x) $BaTiO_3$-x$Ni_{0.6}Zn_{0.4}Fe_2O_4$ composites with grain size distribution

The density of the composites has been calculated by Archimedes principle. The values have been found 3.04 g/cm^3, 3.20 g/cm^3, 3.13 g/cm^3 for x = 0.35, 0.25, 0.15 respectively, i.e., with the increase of NZFO content into the composites, the density increases, but after increasing certain content of NZFO, the density decreases. It is found that 0.75BTO-0.25NZFO composites show the highest density as well as the smallest average grain size. Due to the smaller particle size, better diffusion occurs among the particles during sintering, and as a result, the density is higher.

3.3 Ferroelectric property

The ferroelectricity of BTO-NZFO composites has been examined from the polarization-electric field (P-E) loop. Figure 5 shows the P-E hysteresis loop of (1-x)$BaTiO_3$-x$Ni_{0.6}Zn_{0.4}Fe_2O_4$ composites, where x = 0.15, 0.25 & 0.35. The P-E loops indicate that all samples have weak ferroelectricity, and the obtained oval-shaped ferroelectric loop is called a lossy capacitor hysteresis loop. The values of remnant polarization (Pr), coercivity (Ec) have been measured from the loop, and the values are tabulated in Table 3. It is found that the 85% $BaTiO_3$-15% $Ni_{0.6}Zn_{0.4}Fe_2O_4$ composites have the lowest remnant polarization as well as lowest coercivity, whereas 75% $BaTiO_3$-25% $Ni_{0.6}Zn_{0.4}Fe_2O_4$ composites have the highest remnant polarization and Coercivity value. Chauhan R et al. [24] reported that a higher value of remnant polarization of BTO/NZFO composites is useful for switching applications. However, with a further increase of ferrite content into BTO, the composites' Pr and Ec values decreased. The composites' large coercivity values may be due to the existence of the increased ferrite phase, which usually pins the domain wall motion of the ferroelectric region [1, 25].

The energy density of the BTO/NZFO composites has been calculated from the P-E loop. The energy density (E_d) is the integral area of the P–E loop (charge: lower branch of P–E curve or discharged curve: upper branch of P–E curve), and the y-axis is given by $E_d = \int EdP$ [26], here

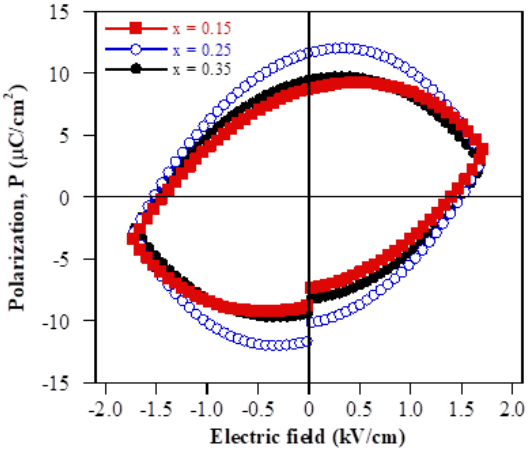

Figure 5 P-E hysteresis loops of (1-x)$BaTiO_3$-x$Ni_{0.6}Zn_{0.4}Fe_2O_4$ composites

E is the applied electric field, and P is the polarization. The calculated charged and discharged values are tabulated in Table 3. It is found that the charged density decreases from 1.1357 to 0.4023 J.cm^{-3} when the NZFO content increases from 15% to 35% in the composites. Thus, the charged density is comparatively lower than the discharged density. However, it is found that the 0.75BTO-0.25NZFO has the highest overall density (charged + discharged density). It may be due to the largest particle size of the said composite. Generally, high dielectric constant, high breakdown strength, low loss, and pore-free dense microstructures are necessary for materials that are to be utilized in high energy density capacitor applications [26].

Table 3 Calculated lattice parameters and crystallite size of (1-x)$BaTiO_3$-x$Ni_{0.6}Zn_{0.4}Fe_2O_4$ composites

Sample	Pr μC/cm^2	Coercivity Ec kV/cm	Charge density (J.cm^{-3})	Discharge density (J.cm^{-3})
0.85BTO-0.15NZFO	8.7319	1.4387	1.1357	7.1665
0.75BTO-0.25NZFO	11.6134	1.5262	0.6552	11.3146
0.65BTO-0.35NZFO	9.4206	1.5048	0.4023	5.3937

3.4 Magnetic properties

The ferromagnetic hysteresis curves (at room temperature) of 0.85BTO-0.15NZFO, 0.75BTO-0.25NZFO and 0.65BTO-0.35NZFO composites are displayed in Figure 6. In contrast, the inset of Figure 6 shows the magnified view of the loops, as mentioned earlier, exhibiting the detailed coercive magnetization field required for the demagnetization of the experimental specimens. The obtained magnetization vs magnetic field (M-H) loops resembled the soft magnetic materials resulting from the existence of ordered magnetic structure of NZFO in the hybrid spinel-perovskite system (BTO-NZFO) [1, 5]. Generally, the ordered magnetic structure is derived from the unbalanced antiparallel spins between the Ni^{2+} ions belonging to the octahedral sites and the Fe^{3+} ions at tetrahedral sites [2].

The measured saturation magnetization (M_s), remnant magnetization (M_r), and coercivity (H_c) of composites are listed in Table 4. It is seen that with increasing the ferromagnetic NZFO phase, all of the magnetic parameters such as M_s, M_r, and $H_c$increase up to 25% NZFO content, but decrease for 35% NZFO compared to 25% NZFO containing composite. B K Bammannavar et al. [3] mentioned the generation of anisotropy layer in the ferrite phase through super exchange interaction of oxygen ions as the principal reason for this kind of magnetization behaviour. According to the theory, the existence of impurity phases at the surface often breaks the super exchange bonds among the magnetic cations. It causes significant surface spin distortion resulting in reduced saturation and remnant magnetization (as observed in 65% BTO:35% NZFO) [27].

However, 0.65BTO-0.35NZFO [M_s= 1.438 emu/g, M_r= 0.090 emu/g, and H_c= 0.160 kOe] still exhibits higher magnetization characteristics compared to 0.85BTO-0.15NZFO [M_s= 0.910 emu/g, M_r= 0.011 emu/g, and H_c= 0.155 kOe]. In the meantime, 0.75BTO-0.25NZFO derives the maximum saturation [M_s= 1.732 emu/g] and remnant magnetization [M_r= 0.025

emu/g] among the synthesized composites. Generally, in the ferrite-ferroelectric system, the ferrite grain is surrounded by ferroelectric grains, which form close contact. Again, the contact increases with increasing ferrite phase, which increases the saturation magnetization and remnant magnetization. But, the presence of more ferroelectric phase (BTO) acts as pores and disrupts the formation of effective magnetic contact resulting in reduced saturation and remnant magnetization as observed in 0.85BTO-0.15NZFO [28].

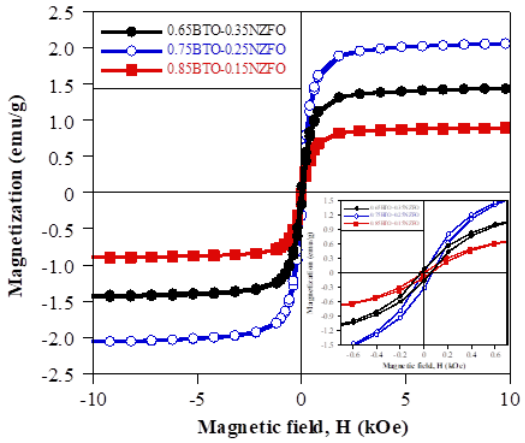

Figure 6 M-H hysteresis loop of (1-x)$BaTiO_3$-x$Ni_{0.6}Zn_{0.4}Fe_2O_4$ composites measured at room temperature

Table 4 Calculated lattice parameters and crystallite size of (1-x)$BaTiO_3$-x$Ni_{0.6}Zn_{0.4}Fe_2O_4$ composites

Compositions	M_s (emu/g)	M_r (emu/g)	M_r/M_s	H_c (kOe)
0.85BTO-0.15NZFO	0.910	0.011	0.012	0.155
0.75BTO-0.25NZFO	1.732	0.025	0.014	0.200
0.65BTO-0.35NZFO	1.438	0.090	0.063	0.160

Again, looking forward to Figure 6, it is observed that the obtained M-H hysteresis loops are in constricted shape, for which these are nominated as 'wasp-waisted.' Generally, materials having grains with broad size distribution and variable coercivities exhibit such kind of hysteresis loops. Besides, superparamagnetic (SPM) particles can contributeto generating such a type of loop. Again, a system consisting of a mixture of a single domain (SD) and superparamagnetic (SPM) particles can also generate this type of 'wasp-waisted' loop if the system has a grain size distribution spreading over a range from the lower to the higher of the threshold limit of SD/SPM. Therefore, fitting M-H loops by following the Langevin function (as given below) gives rise to the term SPM component [29].

$$\mathrm{M} = \mathrm{n}\mu\left\{\coth\left(\frac{\mu\mathrm{H}}{\mathrm{kT}}\right) - \frac{\mathrm{kT}}{\mu\mathrm{H}}\right\} \tag{2}$$

Where μ is magnetic moment per particle ($\mu = M_s V$, M_s is the saturation magnetization and V is the volume of the particle), k is the Boltzmann constant, T is the absolute temperature, and H is the applied field, and n is the number of particles per unit mass.

Figure 7 exhibits the SPM components and the fitted parameters are enlisted in Table 5. From Figure 7, it is observed that the SPM component of 0.75BTO-0.25NZFO rises much higher compared to 0.85BTO-0.15NZFOand 0.65BTO-0.35NZFO. The steepness of the SPM component is completely dependent on μ. However, the μ values for 0.85BTO-0.15NZFO, 0.75BTO-0.25NZFO and 0.65BTO-0.35NZFO are 2.18e-16 emu, 2.38e-16 emu and 2.26e-16 emu, respectively. Hence, 0.75BTO-0.25NZFOexhibited the highest μ value resulting from either larger particle size or higher saturation magnetization.

Considering the particles as spherical shaped, the calculated diameters of the particles of 0.85BTO-0.15NZFO, 0.75BTO-0.25NZFO and 0.65BTO-0.35NZFO composites are 40.88 nm, 41.08 nm and 40.48 nm, respectively. However, the size limit of the SPM particles can be calculated according to the following equation [29]:

$$\mathrm{V} = \frac{25\mathrm{kT}}{\mathrm{K_u}} \tag{3}$$

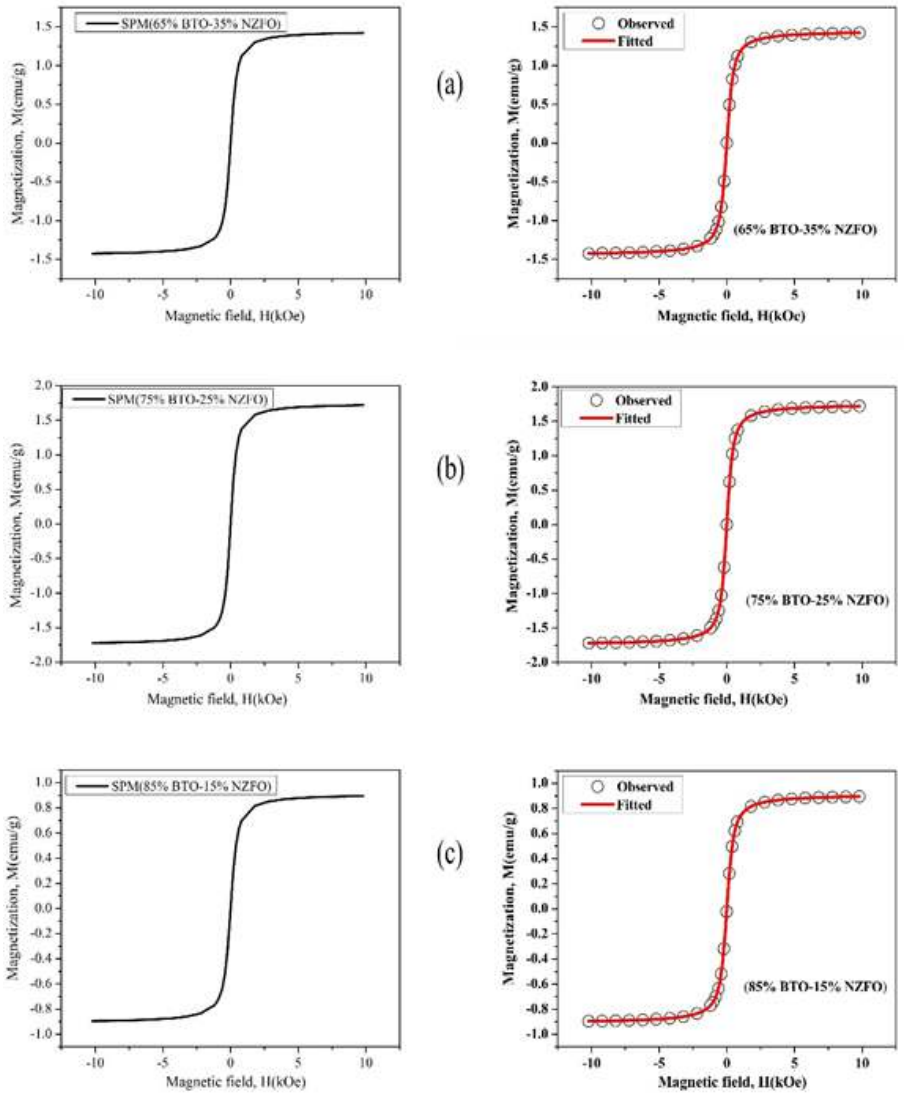

Figure 7 Fitted and SPM component of (a) 65% BTO-35% NZFO, (b) 75% BTO-25% NZFO, (c) 85% BTO-15% NZFO composites.

Where K_u is an effective anisotropy constant which can be estimated through the following equation [30]:

$$H_c = 0.48\frac{2\,K_u}{M_s} \tag{4}$$

The measured critical volume is found to be 9.81e-16 cm^3, 7.54e-16 cm^3, 1.75e-15 $cm^3$for 0.85BTO-0.15NZFO, 0.75BTO-0.25NZFO and 0.65BTO-0.35NZFO, respectively. However, the calculated volumes (0.85BTO-0.15NZFO $\sim$ 3.58e-17 cm^3, 0.75BTO-0.25NZFO $\sim$ 3.63e-17 cm^3, 0.65BTO-0.35NZFO $\sim$ 3.58e-17 cm^3.) of the particles that contribute to the SPM component of the composites remain within the boundary limit which ensures the authenticity of this research work.

Table 5 Fitted magnetic parameters of (1-x)$BaTiO_3$-x$Ni_{0.6}Zn_{0.4}Fe_2O_4$ composites

Composition	μ (emu)	nμ (emu/g)	Calculated Volume (cm^3)	Diameter (nm)	K_u (cm^3)	Critical volume (cm^3)
0.85BTO-0.15NZFO	2.18e-16	0.91	3.58e-17	40.88	1051.67	9.81e-16
0.75BTO-0.25NZFO	2.38e-16	1.75	3.63e-17	41.08	1366.67	7.54e-16
0.65BTO-0.35NZFO	2.26e-16	1.45	3.58e-17	40.48	1051.67	9.81e-16

4 Conclusion

In this research, pure BTO, pure NZFO, and three multiferroic composites (i.e., 0.85BTO-0.15NZFO, 0.75BTO-0.25NZFO, and 0.65BTO-0.35NZFO) were synthesized, and their structural, electrical and magnetic characterization was performed. Each composite exhibited a bi-phasic nature consisting of ferroelectric BTO phase and ferromagnetic NZFO phase. No chemical reaction was proved to be performed during the sintering mechanism. The composites exhibited heterogeneous microstructure without any grain agglomeration. The large coercivity value of the composites [0.85BTO-0.15NZFO $\sim$ 0.155 kOe, 0.75BTO-0.15NZFO $\sim$ 0.200 kOe and 0.65BTO-0.35NZFO $\sim$ 0.160 kOe] was believed to be caused due to the presence of the NZFO phase. However, 0.75BTO-0.15NZFO exhibited the highest overall density (charged + discharged density) [$\sim$ 11.969 J.cm^{-3}] because of the larger grain size [$\sim$ 378.46 nm]. The unbalanced antiparallel spins between the Ni^{2+} ions (in octahedral sites) and the Fe^{3+} ions (in tetrahedral sites) in NZFO developed the ferromagnetic behavior within the composite. The composite exhibited constricted-shaped M-H hysteresis loops because of the existence of SPM and SD particles. The SPM component of 0.75BTO-0.25NZFO raised much higher compared with 0.85BTO-0.15NZFO and 0.65BTO-0.35NZFO. The calculated volumes of the SPM particles remained within the measured critical value, ensuring the originality of this work.However, this research developed a path for utilizing this composite material for ferroelectric and ferromagnetic characteristics.

Conflict of interest and funding

The authors declare that there is no funding source in this research.

Acknowledgements

The corresponding author M. Humayan Kabir is thankful to them who have shared their knowledge and expertise to conduct this research work.

References

[1] Adhlakha N and Yadav KL. Study of structural, dielectric and magnetic behaviour of $Ni_{0.75}Zn_{0.25}Fe_2O_4$-$Ba(Ti_{0.85}Zr_{0.15})O_3$ composites, Smart Materials and Structures, 2012, **21**(11): 115021. https://doi.org/10.1088/0964-1726/21/11/115021

[2] Grigalaitis R, Petrović MMV, Bobić JD, *et al*. Dielectric and magnetic properties of $BaTiO_3$ -$NiFe_2O_4$ multiferroic composites. Ceramic International, 2014, **40**: 6165-6170. https://doi.org/10.1016/j.ceramint.2013.11.069

[3] Bammannavar BK and Naik LR. Electrical properties and magnetoelectric effect in (x)$Ni_{0.5}Zn_{0.5}Fe_2O_4$+(1-x)BPZT composites. Smart Materials and Structures, 2009, **18**(8): 085013. https://doi.org/10.1088/0964-1726/18/8/085013

[4] Adhlakha N, Yadav KL and Singh R. Effect of $BaTiO_3$addition on structural, multiferroic and magneto-dielectric properties of 0.3$CoFe_2O_4$-0.7$BiFeO_3$ceramics. Smart Materials and Structures, 2014, **23**(10): 105024. https://doi.org/10.1088/0964-1726/23/10/105024

[5] Dzunuzovic AS, Petrovic MMV, Bobic JD, *et al*. Magneto-electric properties of x$Ni_{0.7}Zn_{0.3}Fe_2O_4$ -(1-x)$BaTiO_3$ multiferroic composites. Ceramic International, 2018, **44**: 683-694. https://doi.org/10.1016/j.ceramint.2017.09.229

[6] Nan CW, Bichurin MI, Dong S, *et al*. Multiferroic magnetoelectric composites: Historical perspective, status, and future directions. Journal of Applied Physics, 2008, **103**: 031101. https://doi.org/10.1063/1.2836410

[7] Zhu P, Zheng Q, Sun R, *et al*. Dielectric and magnetic properties of $BaTiO_3$/$Ni_{0.5}Zn_{0.5}Fe_2O_4$ composite ceramics synthesized by a co-precipitation process. Journal of Alloys and Compounds, 2014, **614**: 289-296. https://doi.org/10.1016/j.jallcom.2014.06.065

[8] Bammannavar BK and Naik LR. Study of magnetic properties and magnetoelectric effect in (x)$Ni_{0.5}Zn_{0.5}Fe_2O_4$-(1-x)PZT composites. Journal of Magnetism and Magnetic Materials, 2012, **324**: 944-948. https://doi.org/10.1016/j.jmmm.2011.09.016

[9] Rawat M and Yadav KL. Electrical, magnetic and magnetodielectric properties in ferrite-ferroelectric particulate composites. Smart Materials and Structures, 2015, **24**(4): 045041. https://doi.org/10.1088/0964-1726/24/4/045041

[10] Pradhan DK, Puli VS, Tripathy SN, *et al*. Room temperature multiferroic properties of $PbFe_2O_4$ composites. Journal of Applied Physics, 2013, **1141**: 234106-243904. https://doi.org/10.1063/1.484759

[11] Zhang RF, Deng CY and Ren L, *et al*. Dielectric, ferromagnetic and maganetoelectric properties of $BaTiO_3$-$Ni_{0.7}Zn_{0.3}Fe_2O_4$ composite ceramics. Materials Research Bulletin, 2013, **48**: 4100-4104. https://doi.org/10.1016/j.materresbull.2013.06.026

[12] Dzunuzovic AS, Petrovic MMV and Stojadinovic BS, *et al*. Multiferroic (NiZn) Fe2O4-BaTiO3 composites prepared from nanopowders by auto-combustion method. Ceramic International, 2015, **41**: 13189-13200. https://doi.org/10.1016/j.ceramint.2015.07.096

[13] Ashiri R. On the solid-state formation of BaTiO3 nanocrystals from mechanically activated $BaCO_3$ and TiO_2powders: Innovative mechanochemical processing, the mechanism involved, and phase and nanostructure evolutions, RSC Advances, 2016, **6**: 17138-17150. https://doi.org/10.1039/c5ra22942a

[14] Zhou T, Zhang D, Jia L, *et al*. Effect of Ni-Zn Ferrite Nanoparticles upon the Structure and Magnetic and Gyromagnetic Properties of Low-Temperature Processed LiZnTi Ferrites. The Journal of Physical Chemistry C, 2015, **119**: 13207-13214. https://doi.org/10.1021/jp512608z

[15] Sreeja V and Joy PA. Microwave-hydrothermal synthesis of γ-Fe_2O_3 nanoparticles and their magnetic properties. Materials Research Bulletin, 2007, **42**: 1570-1576. https://doi.org/10.1016/j.materresbull.2006.11.014

[16] Jafarzadeh M, Rahman IA and Sipaut CS. Synthesis of silica nanoparticles by modified sol-gel process: The effect of mixing modes of the reactants and drying techniques, Journal of Sol-Gel Science and Technology, 2009, **50**: 328-336. https://doi.org/10.1007/s10971-009-1958-6

[17] Safi R, Shokrollahi H. Physics, chemistry and synthesis methods of nanostructured bismuth ferrite ($BiFeO_3$) as a ferroelectro-magnetic material,Progress in Solid State Chemistry, 2012, **40**: 6-15. https://doi.org/10.1016/j.progsolidstchem.2012.03.001

[18] Li DH, He SF, Chen J, *et al*. Solid-state Chemical Reaction Synthesis and Characterization of Lanthanum Tartrate Nanocrystallites under Ultrasonication Spectra. IOP Conference Series: Materials Scienceand Engineering, 2017, **242**: 012023. https://doi.org/10.1088/1757-899X/242/1/012023

[19] Bekri-Abbes I and Srasra E. Investigation of structure and conductivity properties of polyaniline synthesized by solid-solid reaction.Journal of Polymer Research, 2011, **18**: 659-665. https://doi.org/10.1007/s10965-010-9461-x

[20] Jamal R, Xu F, Shao W, *et al*. The study on the application of solid-state method for synthesizing the polyaniline/noble metal (Au or Pt) hybrid materials. Nanoscale Research Letters, 2013, **8**: 1-8. https://doi.org/10.1186/1556-276X-8-117

[21] Upadhyay SK, Reddy VR and Lakshmi N. Study of (1-x) $BaTiO_3$-x$Ni_{0.5}Zn_{0.5}Fe_2O_4$ (x=5, 10 and 15%) magnetoelectric ceramic composites, Journal of Asian Ceramic Society, 2013, **1**: 346-350. https://doi.org/10.1016/j.jascer.2013.10.001

[22] Jain A, Panwar AK, and Jha AK. Significant enhancement in structural, dielectric, piezoelectric and ferromagnetic properties of $Ba_{0.9}Sr_{0.1}Zr_{0.1}Ti_{0.9}O_3$-$CoFe_2O_4$ multiferroic composites. Materials Research Bulletin, 2018, **100**: 367-376. https://doi.org/10.1016/j.materresbull.2017.12.054

[23] Wurst JC and Nelson JL. Two-Phase Polycrystalline Ceramics.Journal of American Ceramic Society, 1972, 46.

[24] Chauhan R andSrivastava RC. Various properties of the 0.6$BaTiO_3$-0.4$Ni_{0.5}Zn_{0.5}Fe_2O_4$ multiferroic nanocomposite. Pramana - Journal of Physics, 2016, **87**: 2-7. https://doi.org/10.1007/s12043-016-1263-1

[25] Rawat M and Yadav KL. Dielectric, ferroelectric and magnetoelectric response in $Ba_{0.92}(Bi_{0.5}Na_{0.5})_{0.08}TiO_3$-$Ni_{0.65}Zn_{0.35}Fe_2O_4$ composite ceramics. Smart Material and Structures, 2014, **23**(8): 085032. https://doi.org/10.1088/0964-1726/23/8/085032

[26] Puli VS, Pradhan DK, Chrisey DB, *et al*. Structure, dielectric, ferroelectric, and energy density properties of (1-x)bzt-xbct ceramic capacitors for energy storage applications, Journal of Material Science, 2013, **48**: 2151-2157. https://doi.org/10.1007/s10853-012-6990-1

[27] Nathani H, Gubbala S and Misra RDK. Magnetic behavior of nanocrystalline nickel ferrite: Part I. The effect of surface roughness, Materials Science and Engineering: B, 2005, **121**: 126-136. https://doi.org/10.1016/j.mseb.2005.03.016

[28] Kambale RC, Shaikh PA, Bhosale CH, *et al*. Studies on magnetic, dielectric and magnetoelectric behavior of (x)$NiFe_{1.9}Mn_{0.1}O_4$ and (1-x)$BaZr_{0.08}Ti_{0.92}O_3$ magnetoelectric composites. Journal of Alloys and Compounds, 2011, **48**: 310-315. https://doi.org/10.1016/j.jallcom.2009.09.080

[29] Cullity GBD. Introduction to Magnetic Materials, John Wiley & Sons, Ltd., 2011.

[30] Stoner EC. A mechanism of magnetic hysteresis in heterogenous alloys. Philosophical Transactions of the Royal Society A, 1948, **826**: 599-642.